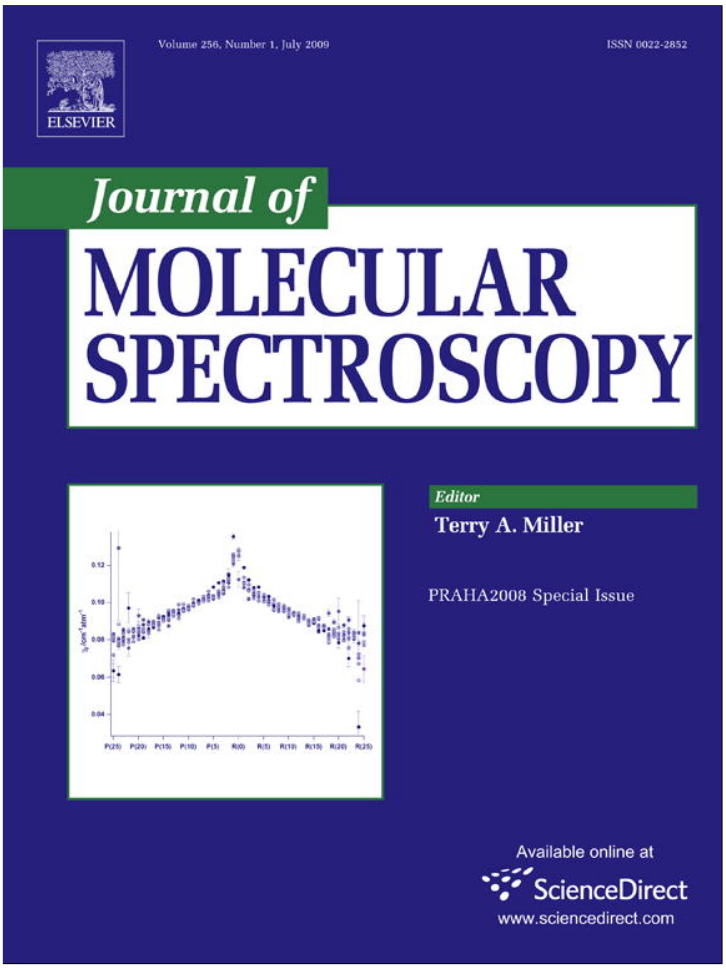

Journal of Molecular Spectroscopy 256 (2009) 152–162

Contents lists available at ScienceDirect

Journal of Molecular Spectroscopy

journal homepage: www.elsevier.com/locate/jms

Interactions between vibrational polyads of propyne, $H_3C—C\equiv CH$: Rotational and rovibrational spectroscopy of the levels around 1000 cm^{-1}

P. Pracna [a,*], H.S.P. Müller [b], Š. Urban [c], V.-M. Horneman [d], S. Klee [e]

[a] J. Heyrovský Institute of Physical Chemistry, v.v.i., Academy of Sciences of the Czech Republic, Dolejškova 3, 18223 Prague 8, Czech Republic
[b] I. Physikalisches Institut, Universität zu Köln, Zülpicher. Str. 77, 50937 Köln, Germany
[c] Department of Analytical Chemistry, Institute of Chemical Technology, 16628 Prague 6, Czech Republic
[d] Department of Physical Sciences, University of Oulu, B.O.X. 3000, 90014 University of Oulu, Finland
[e] Institut für Physikalische Chemie, Justus-Liebig-Universität Gießen, Heinrich-Buff-Ring 58, 35392 Gießen, Germany

ARTICLE INFO

Article history:
Received 10 February 2009
In revised form 7 April 2009
Available online 22 April 2009

Keywords:
Methylacetylene
High resolution
FTIR spectroscopy
Submillemeter-wave spectroscopy

ABSTRACT

The study of vibration resonance physics in propyne is based on experimental measurements of about 600 new rotational transitions between 495–590 and 700–760 GHz in excited vibrational levels $v_5 = 1$, $v_8 = 1$, $v_{10} = 3$ and $v_9 = v_{10} = 1$ with vibrational energies around 1000 cm^{-1}. The limits to the assignments and analysis were imposed by as yet unresolved anharmonic resonances with the states of the next higher polyad of levels lying above 1200 cm^{-1}, which affect the rotational states involved in transitions that would be measurable with non-vanishing intensities. Vibration–rotation spectra pertaining to the levels in question were studied in the regions 880–1150 cm^{-1} (the ν_5 and ν_8 fundamental bands), 550–750 cm^{-1} (the $v_9 = v_{10} = 1 \leftarrow v_{10} = 1$ hot bands) and 250–400 cm^{-1} (the $v_{10} = 3 \leftarrow v_{10} = 2$ "superhot" bands). A simultaneous least-squares fit of both types of data provides their reliable but in the case of accurate rotational data not always fully quantitative reproduction.

1. Introduction

Propyne, also known as methylacetylene ($H_3C—C\equiv CH$), is a symmetric-top molecule of astrophysical and astrochemical importance with a carbon chain that exhibits low-frequency bending vibrations. The fundamental bands of these vibrations (ν_9 at 639 cm^{-1} corresponding to $\equiv$C—H bending and ν_{10} at 331 cm^{-1} corresponding to C—C$\equiv$C bending) were clearly observed in the spectra of Titan [1]. Its strongly prolate geometry makes this molecule an ideal probe of the kinetic temperature of the interstellar medium [2] because of its closely spaced rotational lines belonging to states with different values of the *K* rotational quantum number whose excitation temperature varies rapidly with *K*. For this reason, this molecule has been investigated extensively not only in infrared studies but also using microwave and millimeter wave spectroscopy (see e.g. Ref. [3] and the references therein).

The inclusion of highly accurate rotational data into simultaneous analyses with vibration–rotation data always represents a stringent test of the accuracy of vibration–rotation Hamiltonians used in the description of molecular energy levels. In the case of propyne, the traditional approach of dividing the rovibrational analyses into studies of isolated clusters (polyads) of vibrational levels connected by resonances, as illustrated in Fig. 1, started to reveal problems of accurate reproduction of data once the transition frequencies pertaining to higher *K* states were included, especially those from microwave and millimeter wave measurements. One indication of such poor convergence of the rovibrational Hamiltonian was observed already in an early study of the lowest fundamental level $\nu_{10} = 1$ [4], where it was considered as a truly isolated state.

The isolated polyad approach was used as well in our previous studies of the cluster of levels around 1000 cm^{-1} (the 1000-cluster) [5,6], which, besides the combination (C0 and C2, for short) and overtone (O1 and O3) levels of the two lowest frequency modes ν_9 and ν_{10}, includes two other fundamental levels $v_5 = 1$ (F5, C—C stretching) and $v_8 = 1$ (F8, CH_3 rocking).[1] The goal of these earlier works was to combine rovibrational data with newly measured rotational transitions up to 360 GHz and analyze them with a model including all the relevant interactions in the 1000-cluster. In the calculations, we were still left with problems of the rapid loss of data-reproduction accuracy with growing *K* and were unable to make the fits converge better within the model of an isolated polyad. Since at this stage we still had the energies of the combination and overtone levels calculated from the hot and "superhot" band transitions originating from the lower levels $\nu_{10} = 1$ and 2, we were led to have them reanalyzed first, again with the vastly extended measurements of the rotational data [7,8]. These studies revealed the role of

[1] For the sake of brevity, we are using the 'shorthand' notation for vibrational levels introduced in Ref. [5]. For details the reader should refer to Table 1 of the original paper and tables with fitted parameters of the present one.

* Corresponding author. Fax: +420 28658 2307.
E-mail address: pracna@jh-inst.cas.cz (P. Pracna).

0022-2852/$ - see front matter © 2009 Elsevier Inc. All rights reserved.
doi:10.1016/j.jms.2009.04.003

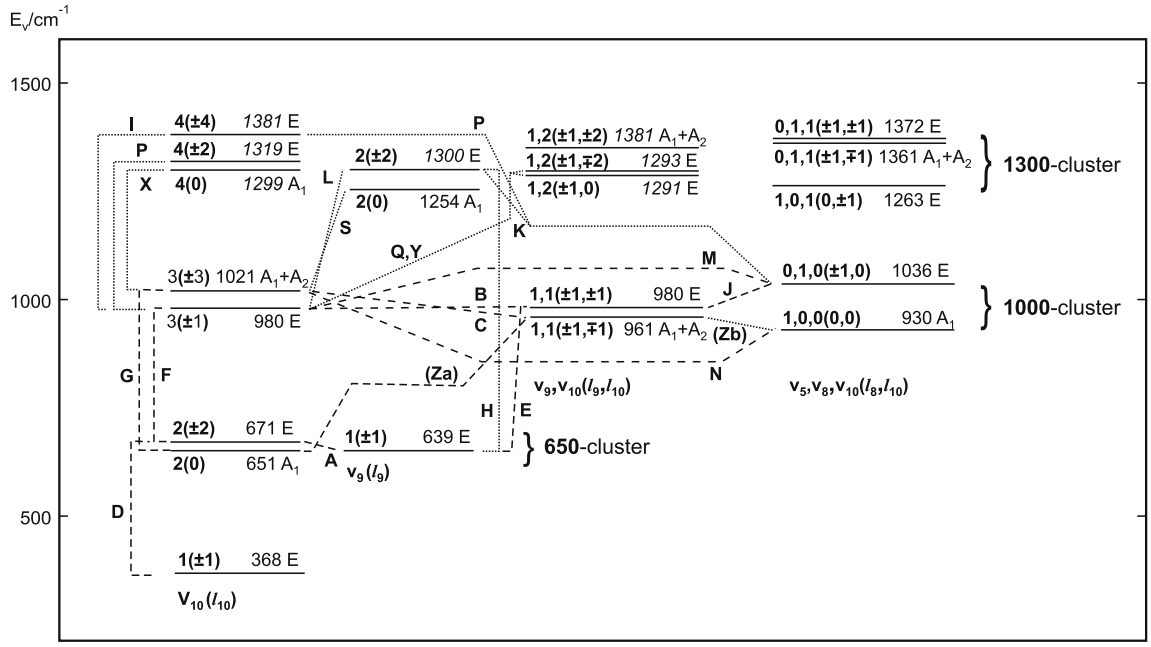

Fig. 1. The lowest clusters of vibrational levels of propyne with the vibrational energies and symmetries as well as the resonant anharmonic interactions indicated. The fitted ones are drawn with dashed lines, the neglected ones with dotted lines. The resonances are denoted with labels corresponding to the more detailed Fig. 2.

anharmonic resonances among the clusters of levels in much more detail and indicated the problems that should be anticipated in studies of the higher clusters.

For an overview of the richness of anharmonic interactions among the low-lying vibrational levels, we introduce here with advantage the diagram of the "purely *K*-dependent reduced" energies given in Fig. 2. It shows vibration–rotation energies with all but the purely *K*-dependent terms subtracted. In addition, we have also subtracted the value of $(A-B)_0K^2$ from these energies to remove the rapid variation of energies with *K*, common to all the levels. This kind of reduced energies, given in the first approximation by

$$E_{red}(K,l) = E_v + [(A-B)_v - (A-B)_0]K^2 \mp 2(A\zeta)_v Kl, \quad (1)$$

has an advantage in its illustrative manner of visualizing the occurrence of local Fermi (or higher anharmonic) resonances between levels with the same value of *K*. Such resonances can occur between states with the sum of vibrational angular momentum quantum numbers *l* differing by $\pm 3n$ ($n = 0, 1, \ldots$), which follows from the general condition for non-vanishing Hamiltonian matrix elements in C_{3v} symmetric-top molecules $\Delta(k - \sum l) = \pm 3n$. This separates the levels of vibrational symmetry *E* shown in Fig. 2a from those of vibrational symmetries A_1 and A_2 shown in Fig. 2b.

In the former diagram we can immediately recognize a cubic anharmonic (Fermi) resonance due to the close coincidence of the $v_9 = 1$ fundamental and the $v_{10} = 2$ overtone levels in the 650-cluster. It is sharply localized to the states with $K = 1$ of the $v_9 = 1^{-1}$ and $v_{10} = 2^{+2}$ sublevels (denoted as resonance A in Fig. 2a). An analogous resonance occurs in the 1000-cluster for the states with one more v_{10} quantum excited. In fact, there are two such resonances between the sublevels of the combination/overtone states $v_9 = 1^{+1}$, $v_{10} = 1^{+1}/v_{10} = 3^{-1}$ occurring at $K = 0$, denoted as resonance B in Fig. 2a, and $v_9 = 1^{-1}$, $v_{10} = 1^{+1}/v_{10} = 3^{+3}$ at $K = 2$, resonance C in Fig. 2b. These three resonances have been included in previous analyses, but it was noted already in the earlier paper [9] that the ratio of the coupling terms of resonances B and C differed by more than 20% from the values predicted from the resonance term A. This was an indication of the still effective representation of these anharmonic coupling terms, even when only the lowest *K* states were studied.

The origin of the problems with handling the rich variety of anharmonic resonances lies in the strongly prolate geometry of propyne with a large value of the *A* rotational constant ($\sim$5.31 cm^{-1}) and the nature of the two lowest bending modes, which are both degenerate (E symmetry) vibrations and have large values of the *z*-Coriolis constants ζ_t^z, being about 0.9 in the v_{10} mode and very close to 1.0 in the v_9 mode. This makes the $+l$ and $-l$ levels of such vibrational states quickly diverge and approach levels of the neighboring clusters. Even though vibrational energies in the clusters differ by about 300 cm^{-1}, resonant crossings due to cubic and quartic anharmonic interactions occur, when sufficiently high values of *K* are reached.

Such a resonance between the $v_{10} = 1^{-1}$ and $v_{10} = 2^{+2}$ sublevels at $K = 12$ (resonance D) was the main reason for the convergence problems of the vibration–rotation Hamiltonian and the poor reproduction of the high-*K* data in an earlier study of the $v_{10} = 1$ level [4], where it had been neglected. With the help of extended measurements of the rotational transitions, we were able to fit the Fermi interaction term [7], despite only an approximate extrapolation of the $v_{10} = 2^{+2}$ levels based on the constants from an earlier study [10]. A complete assignment and quantitative reproduction of the rotational MMW data in the region of this Fermi resonance was accomplished later in line with the study of the cluster of the $v_9 = 1$ and $v_{10} = 2$ levels [8], for which several hundred new MMW transitions were systematically measured between 85 and 920 GHz.

It is obvious that also this Fermi resonance is propagated to higher polyads by adding one or more quanta of excitation of the v_{10} mode or a quantum of the v_9 mode, just like in the case of the previously mentioned A, B, C resonant crossings. Two of them can be immediately spotted in Fig. 2a and another one in Fig. 2b. They produce resonance couplings between the 650- and 1000-clusters. They occur between $v_9 = 1^{-1}/v_9 = 1^{+1}$, $v_{10} = 1^{+1}$ (resonance E) and $v_{10} = 2^{-2}/v_{10} = 3^{+1}$ (resonance F), both at $K = 11$, and between $v_{10} = 2^0/v_{10} = 3^{+3}$ at $K = 13$ (resonance G).

The values of these Fermi terms were determined in the analysis of the 650-cluster [8], but were found to suffer from effectivity like in the case of resonances A, B, C. This effectivity could not be removed by an improved description of the 1000-cluster in the

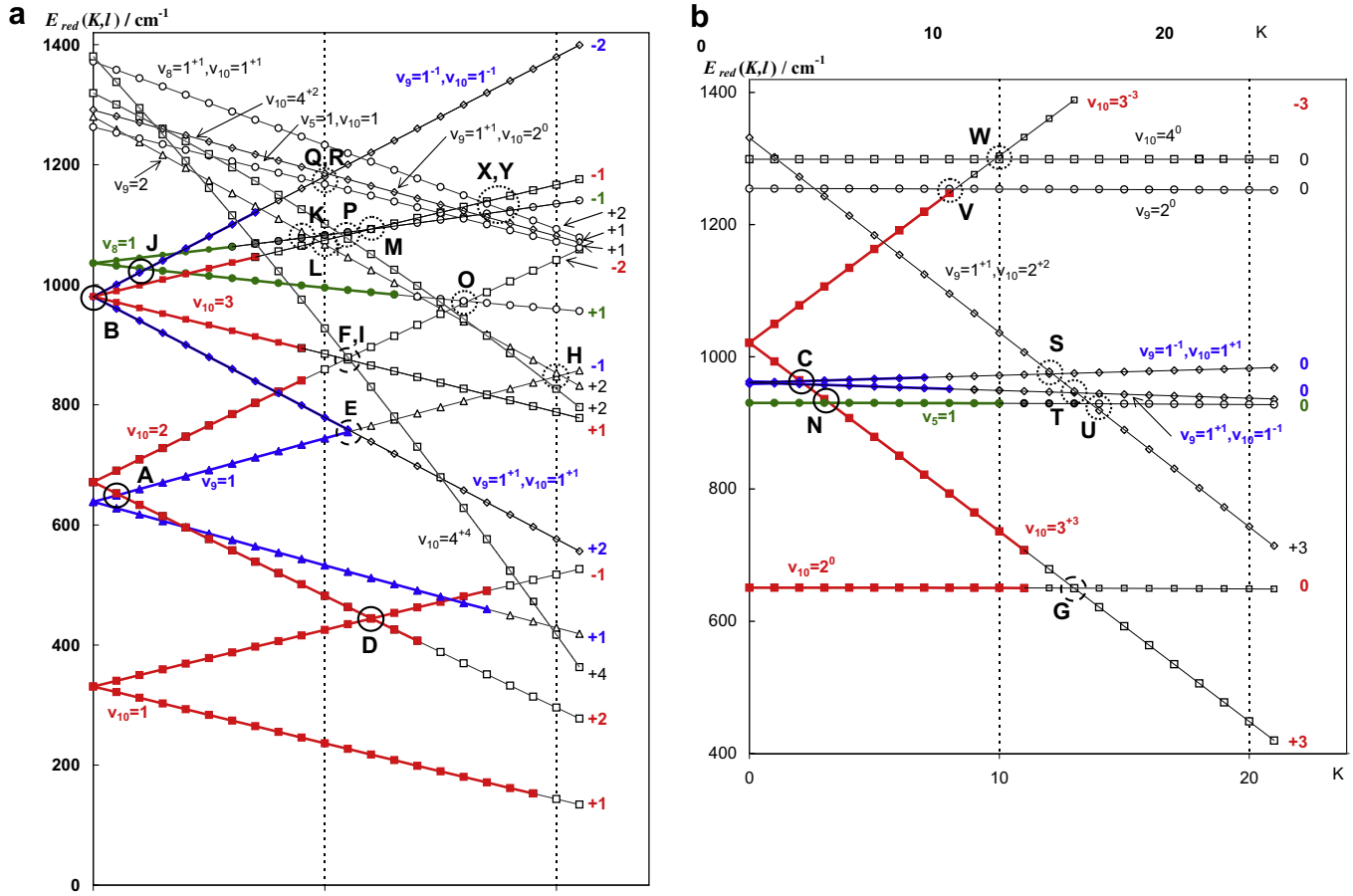

Fig. 2. Diagrams of the purely *K*-dependent reduced energies of the levels belonging to the states of vibrational symmetry E (a) and symmetries A_1 and A_2 (b) with the local anharmonic resonances marked with circles. The resonances determined quantitatively are shown in full circles, whereas those being still only effective in dashed ones. The resonances neglected in the present study are shown as dotted circles. The levels, for which experimental data were assigned and included in the analyses, are shown as full black symbols (colour symbols in online). The levels which were assigned but not included in the fitting because of their poor reproduction are shown as grey symbols. Each series of levels is marked with its *l* quantum number on the right hand side of the diagrams.

present study because we were not able to resolve all the anharmonic resonances within this cluster. This is a consequence of anharmonic interactions with the higher 1300-cluster from which the levels obviously penetrate not only into the 1000-cluster but also as low as the 650-cluster. Two examples of the latter resonances are H and I in Fig. 2a. Resonance H, analogous to D, couples the fundamental level $v_9 = 1^{-1}$ with $v_9 = 2^{+2}$ with the crossing estimated to occur at $K = 20$. The second resonance I with $v_{10} = 3^{+1}$ is estimated to occur because of a steep descent of the $v_{10} = 4^{+4}$ sublevel at the much lower value of $K = 11$ and coincide with resonance F.

The presence of fundamental levels F5 and F8 in the 1000-cluster produces several new types of anharmonic resonant crossings within this cluster (J–N in Fig. 2) as well as one more with the lower 650-cluster (resonance O). In particular, the coincidence of three anharmonic resonances K, L, M on the $l = -1$ side of F8 (and an additional one, P, with the 1300-cluster) makes the reproduction of data pertaining to this sublevel of F8 very problematic. It is apparent from Fig. 2 that there are several more anharmonic resonances (Q–W) that occur in the vicinity of the available experimental data of the 1000-cluster for *K* between 8 and 14. The list of anharmonic resonances with the 1300-cluster also includes resonances X and Y with the combination level $v_8 = 1^{+1}$, $v_{10} = 1^{+1}$. In such a situation, it becomes quite obvious that any attempt to adjust the unknown resonant terms, for which the experimental data were measured only below the resonances, can hardly lead to meaningful results because of the multi-dimensional character of the anharmonic couplings.

It is, however, questionable whether an analysis of the full 1300-cluster would lead to a "disentanglement" of such a system of numerous anharmonic couplings. Besides the levels which originate from the 1000-cluster by adding one quantum of the v_{10} vibration and the 650-cluster by adding one quantum of the v_9 vibration, this cluster contains two other fundamental levels $v_4 = 1$ (symmetric CH_3 bending) and $v_7 = 1$ (asymmetric CH_3 bending). The existing experimental information for this cluster is only sparse. It comprises IR studies of the latter two fundamental levels, the $v_9 = 2^0$ sublevel, the $v_5 = v_{10} = 1$ combination level, and part of the $v_8 = v_{10} = 1$ combination level [11,12]. There also exists a very limited set of microwave data for the low-*K* transitions in the $v_{10} = 4$ and $v_9 = 2$ vibrational states [13,14]. Gathering a complete set of experimental data, at least for the lower *K* levels of all vibrational levels of this cluster, which would allow a somewhat less effective modeling of the resonant crossings with the 1000-cluster, is limited by the sensitivity of the conventional FTIR and MMW experiments, because these were more or less reached in the study of the 1000-cluster.

Therefore, we accept that the present analysis of the 1000-cluster does not quite achieve a quantitative reproduction of the large body of experimental data which are summarized in Table 1. It represents a compromise between a description of the well established local resonances (not only anharmonic) occurring for

Table 1
Summary of the experimental data used in the analysis with the range of rotational levels, experimental accuracy, and standard deviation of reproduction.

Type of data	No. of data[a]	Upper limit of J	Upper limit of K[b]	Experimental accuracy[c]	Standard deviation[c]
$v_5 = 1$ (IR)	1183	65	10	0.20	0.37
$v_8 = 1$	2050	60	6/13	0.20	0.22
$v_9 = 1^{\pm1}$, $v_{10} = 1^{\mp1}$	1972	60	9 (10)/7	0.30	0.38
$v_9 = 1^{\pm1}$, $v_{10} = 1^{\pm1}$	2488	65	7/11	0.30	0.29
$v_{10} = 3^{\pm1}$	1520	60	6/7	0.30	0.22
$v_{10} = 3^{\pm3}$	1795	60	6/9	0.30	0.20
$v_5 = 1$ (rot)	144	43	9 (12)	10–50	126
$v_8 = 1$	209	43	7 (11)/13	10–50	71
$v_9 = 1^{\pm1}$, $v_{10} = 1^{\mp1}$	207	43	8/6 (8)	10–50	119
$v_9 = 1^{\pm1}$, $v_{10} = 1^{\pm1}$	229	43	7/9	10–50	133
$v_{10} = 3^{\pm1}$	210	43	7 (8)/9	10–50	135
$v_{10} = 3^{\pm3}$	204	43	7 (8)/11	10–50	122

In the combination level $v_9 = v_{10} = 1$ the $-l/+l$ levels correlate with the sign of l_{10}. Values in parentheses represent levels assigned but not included in fitting.
[a] Data with nonzero weights.
[b] In a degenerate vibrational state the two values correspond to the $-l/+l$ levels.
[c] In 10^{-3} cm^{-1} units for IR data, in kHz units for rotational data.

lower K rotational states and the increasingly effective treatment of only some of the anharmonic resonances with onset from $K \geqslant 10$. It provides reliable assignments of an extensive set of more than 1200 rotational transitions consistent with the more than 9600 vibration–rotation transitions assigned in IR spectra.

It is worthwhile mentioning that a similar investigation of the interactions between vibrational polyads has been started fairly recently for the related methyl cyanide molecule CH_3CN [15], in which the CH moiety of propyne has been replaced by the N atom. This leads to one non-degenerate and one doubly-degenerate vibration less when compared with propyne. In particular, the mode corresponding to v_9 is missing in methyl cyanide. This leads to a somewhat simpler vibrational structure especially at lower energies.

2. Experimental details

The submillimeter wave (SMMW) spectra were recorded with the Cologne Terahertz Spectrometer that has been described in detail elsewhere [16,17]. Phase-locked backward wave oscillators (BWO's; ISTOK Research and Production Company, Moscow Region, Russia) were used as sources in selected regions between 495 and 760 GHz. A magnetically tuned, liquid He-cooled InSb hot electron bolometer was employed as the detector. A 3.5-m long glass absorption cell, kept at room temperature, was used in the static mode and filled with fresh sample every 10–30 min at pressures of 1–4 Pa, adjusted according to the strength of the absorption lines. The estimated uncertainties of 10–50 kHz were based on the line shapes and the signal to noise ratios. The studies of the rotational spectra of H_2CO [18] and SO_2 [19] are two examples of achievable accuracies in this laboratory.

FTIR spectra from three regions were used for assigning the vibration–rotation transitions. The fundamental bands v_5 and v_8 were assigned from a spectrum used previously for preliminary assignments in the v_5 fundamental band [8]. This FTIR spectrum was recorded in Giessen in the range of 860–1250 cm^{-1}, using a multipass White-type cell with a path length of 19.54 m and KBr windows, at room temperature (299–300 K), employing a mid-IR globar source and a liquid helium cooled GeCu detector. This spectrum was recorded at a resolution (defined as 1/maximum optical path difference) of 0.0028 cm^{-1} and a pressure of 400 Pa, with 1000 scans accumulated.

The combination level $v_9 = v_{10} = 1$ was studied from the hot bands originating in the lowest excited vibrational $v_{10} = 1$ state, falling thus into the region of the v_9 fundamental band. The FTIR spectra were measured in the range of 560–840 cm^{-1} with the same experimental setup as above, with the resolution increased to 0.0018 cm^{-1}. Of the three spectra recorded at pressures of 4, 40, and 400 Pa with 280, 100, and 270 scans accumulated, respectively, the first two were used in our study. The calibration of the Giessen FTIR spectra was done with N_2O [20] at pressures of 4 and 3 Pa for the regions of the v_9 band and the v_5 and v_8 bands, respectively.

The overtone level $v_{10} = 3$ was studied from the hot bands originating in the vibrational level $v_{10} = 2$. We exploited a spectrum from the region of 285–365 cm^{-1} used previously in the study of the v_{10} fundamental band [7]. This spectrum was recorded in the Max laboratory of the University of Lund in Sweden, using a White-type cell [21] with a 6.4-m pathlength and KRS-5 windows, synchrotron radiation as a source of the Bruker IFS 120 FT spectrometer, and a silicon bolometer as the detector, at a pressure of 40 Pa and room temperature. The bolometer was provided with a cold low-pass filter with the cutoff wavenumber at 360 cm^{-1}. A 6 mm Mylar beamsplitter was used. The resolution owing to the maximum optical path difference was 0.00085 cm^{-1} with the registration time being 25 h. This spectrum was calibrated with H_2O lines [22].

3. Theoretical model

The vibration–rotation Hamiltonian used for fitting the experimental data was essentially the same as in the two previous studies of the 1000-cluster [5,6]. The only significant modification was the inclusion of the terms of the anharmonic couplings with the 650-cluster (resonances E, F, G). This resulted in somewhat different values of the fitted vibrational energies and in smaller extents of the axial constants A, D_K, and H_K. The diagonal part of the effective vibration–rotation Hamiltonian has been used in the expansion up to the sextic terms. The new rotational data contributed to a vastly improved determination of the quartic centrifugal distortion terms. Although the sextic centrifugal distortion constants were also determined with much smaller statistical errors than previously [8], they still remain quite effective. We accept that with regard to the newly introduced anharmonic coupling terms and many other, not only anharmonic ones, still neglected. Like in all previous studies of lower vibrational levels, it was not possible to keep them fixed to the ground state values, because that would deteriorate the fit dramatically. Besides the dominant anharmonic couplings, there are numerous Coriolis, α-resonance, and l-type interactions between the levels of the 1000-cluster. A detailed description of their effects is given in the next section with the discussion of the results of fitting for the individual vibrational states.

An overview of the Hamiltonian matrix elements used in the present analysis is collected in Appendix A. The least squares fits were performed with the SIMFIT program [23], in which the experimental data were given statistical weights proportional to the inverse squares of their estimated experimental errors. Thanks to an interactive lower state combination difference (LSCD) checking the assignments in the IR spectra [24], we were able to assess the accuracy of individual lines efficiently. It was the case for the hot bands in particular that only a fraction of the nonoverlapping lines in congested regions could have been attributed the ideal accuracy estimated from the true experimental one.

4. Results and discussion

4.1. Fundamental levels $v_5 = 1$ and $v_8 = 1$

The two fundamental levels were naturally the first from the 1000-cluster studied by infrared spectroscopy [25]. Later, microwave spectra in the F5 level were recorded [26], showing the possibility of extending the rotational measurements to the region of vibrational states around 1000 cm^{-1}. This led to a systematic investigation of all the levels in this cluster by rotational spectroscopy, first in the region up to 105 GHz ($J = 5$) and later up to 360 GHz ($J = 20$). These rotational data were simultaneously analyzed with the previously measured infrared data of the v_5 and v_8 bands and with a provisional representation of the remaining levels of the 1000-cluster [5]. Subsequently, rotational spectra in the combination $v_9 = v_{10} = 1$ level and the overtone $v_{10} = 3$ level were analyzed with a completed assignment of the hot IR band transitions to these levels, treating the 1000-cluster in a global fit for the first time [6].

With the aim of making the picture of this vibrational cluster with complex interactions more complete, we extended the measurements of rotational spectra for the purpose of this analysis up to 760 GHz ($J = 42$) and also remeasured both fundamental rovibrational bands. This extended the data set to 144 and 209 rotational transitions and almost 1200 and over 2000 rovibrational transitions pertaining to the F5 and F8 levels, respectively.

As the vibrational F5 state is nondegenerate, it does not exhibit any anharmonic resonance crossing with the lower 650-cluster, because no level with a considerable $A\zeta$ splitting term is available (cf. Fig. 2b). The only level which bridges the gap of about 300 cm^{-1} is the $v_{10} = 2^{-2}$ sublevel, producing a resonant crossing with F5 due to a weak q_{12} ($\Delta k = +1, \Delta l = -2$) interaction with a very localized effect, which was already analyzed in the previous study [8].

Within the 1000-cluster, an anharmonic (quartic) crossing of the levels F5 with the levels of O3 occurs for the value of $K = 3$ (resonance N). Fig. 2b also shows that the levels of F5 are closely followed by those of the C0 combination level. The combination level has only a small $A\zeta$ splitting term and thus no resonant crossing occurs. The effect of this anharmonic interaction is discussed in the following subsection in the context of the other anharmonic resonances pertaining to the $v_9 = v_{10} = 1$ combination level.

Fig. 2b also explains the difficulties with fitting the high-K rotational data ($K \geqslant 10$) of F5 accurately because of the approaching crossing with the $v_9 = 1^{+1}$, $v_{10} = 2^{+2}$ level at $K = 14$. It was not possible to make any adjustment of this anharmonic term for two reasons. First, the uncertainties of energies of the so far unanalyzed $v_9 = 1^{+1}$, $v_{10} = 2^{+2}$ rovibrational levels would be very high if we included this level in our model without analyzing the $v_9 + 2v_{10}$ combination band (i.e. using some estimation of its constants from the analysis of the $v_9 = 1$ and $v_{10} = 2$ levels). In addition to this, another resonant crossing due to a second-order Coriolis interaction ($\Delta k = -1, \Delta l = +2$) with the $v_9 = 2^{+2}$ level is estimated to occur for $K = 13$ of F5. Therefore we set zero weights in the fits to the rotational data with $K \geqslant 10$, in order to maintain good reproduction of the F5 data, although there is no doubt about the correctness of their assignments. Such a coincidence of anharmonic and Coriolis couplings is typical for higher-K levels of almost all the vibrational states of propyne. It was first described in the analysis of the fundamental level F10 [7], where the fitting of the Coriolis coupling with F9 became possible only after an accurate determination of the anharmonic coupling between $v_{10} = 1^{-1}$ and 2^{+2} (resonance D).

There is another weak interaction coupling the F5 level to the F8 through an α-resonance term. Although the crossing of levels (between $K = 5$ and 6 of $v_5 = 1$ and $K = 3$ and 4 of $v_8 = 1^{+1}$) does not bring the levels closer than about 10 cm^{-1}, its effect was detected in the rotational spectra and the addition of the corresponding, well-determined term improved the fit.

The anharmonic perturbations of the fundamental level F8 are more complex, because it is a degenerate vibrational level and therefore has more potential interaction partners with significantly large $A\zeta$ splitting terms. The reproduction of data in the lower sublevel $v_8 = 1^{+1}$ was maintained without problems up to $K = 13$, where the assignments were terminated because of the vanishing intensities in both the rotational and rovibrational spectra. This was still sufficiently away from the resonance O with $v_{10} = 2^{-2}$ at $K = 16$. The typical patterns of the ${}^rQ$-branches up to $K = 12$ are clearly visible in the overview of the v_8 band in Fig. 3. All interactions pertaining to these $+l$ levels are well determined and the corresponding data are reproduced more or less within their experimental accuracy. The strongest perturbation in the $v_8 = 1^{+1}$ sublevel is a Fermi resonance with the $v_9 = 1^{-1}$, $v_{10} = 1^{-1}$ component of the combination level with the closest approach of about 7 cm^{-1} occurring for $K = 2$. The $K = 2$ level of $v_8 = 1^{+1}$ is involved in two other weaker interactions, namely a second-order Coriolis ($\Delta k = +1, \Delta l = -2$) with the $K = 3$ level of $v_{10} = 3^{-1}$ and an α-resonance ($\Delta k = +2, \sum \Delta l = -1$) with the $K = 4$ level of $v_9 = 1^{-1}$, $v_{10} = 1^{+1}$. An effect of the latter resonance can be seen clearly in the expanded ${}^rQ_1$-branch shown as the lower trace in Fig. 3. This resonance produces several newly assigned perturbation-allowed transitions of the ${}^tQ_1$-branch with a selection rule $\Delta k = +3$, formally belonging to the combination band $v_9 + v_{10}$.

The other sublevel $v_8 = 1^{-1}$ is free from perturbations only at lower K values. From $K = 9$ upwards, we find coincidences of four anharmonic resonances, from which only one (M) is a resonance within the 1000-cluster. The resonance crossing with $v_{10} = 3^{-1}$ occurs at $K = 12$. The remaining three resonances couple the levels of the 1000-cluster to the 1300-cluster. Two of them are due to the level $v_9 = 2^{+2}$ which first crosses $v_8 = 1^{-1}$ at $K = 9$ (resonance K) and then also the $v_{10} = 3^{-1}$ at $K = 10$ (resonance L). The fourth one (P) is due to a crossing of $v_{10} = 3^{-1}$ with $v_{10} = 4^{+2}$ occurring at $K = 11$. This was a reason why we were not able to fit the data pertaining to the levels of $v_8 = 1^{-1}$ for $K \geqslant 7$. We measured and tentatively assigned the rotational data for levels up to $K = 11$, but these could not be included into the fits when the mentioned resonances were neglected. Their assignments were increasingly uncertain at higher K and they would not be of help for determining the respective resonance terms as we could not combine the rotational with IR data. Although we already had the Loomis–Wood assignment program with interactive LSCD checking at our disposal at this point, the available spectrum turned out to be too weak in this region because of significant intensity depletion, obviously because of these anharmonic resonances. The intensity asymmetry between the $\Delta l = +1$ and -1 parts of the spectrum can be clearly seen in Fig. 3. While the ${}^rQ$-branches were easily followed up to $K'' = 12$ together with the corresponding ${}^rR$-branches, we were able to assign the ${}^pQ$-branches only up to $K'' = 6$. The ${}^pQ_7$-branch was already very weak and its J-assignment ambiguous because of the vanishing intensities of the corresponding ${}^pP$-branch, necessary for LSCD checking.

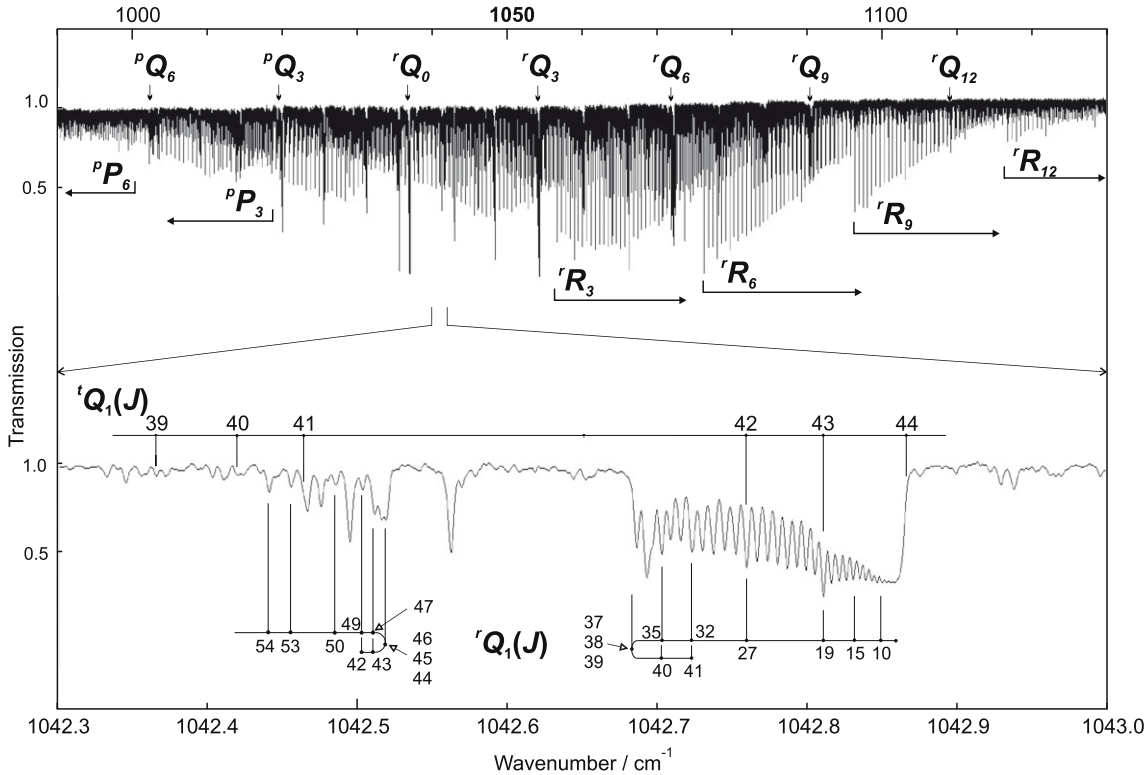

Fig. 3. Overview of the ν_8 band (upper trace) with the prominent patterns of the $^{p,r}Q$, ^pP, and ^rR branches indicated. The effect of the resonance crossing due to an α-resonance on the expanded $^rQ_1$-branch with the emergence of perturbation-allowed transitions is shown as the lower trace.

The $v_9 = 2^{+2}$ and $v_{10} = 4^{+2,+4}$ sublevels descending from the higher 1300-cluster caused major problems when their anharmonic interactions with the currently studied states were neglected. This will be discussed in the following subsection in connection with the still very effective representation of resonances E and F.

4.2. Combination level $v_9 = 1$, $v_{10} = 1$ and overtone level $v_{10} = 3$

A common feature of both these levels is that the corresponding combination and overtone bands from the vibrational ground state are weak and that they were assigned with preference from the hot bands with the $v_{10} = 1$ and 2 levels as lower states. This was a reason why in earlier stages of the analyses [5,6] we had in fact more complete information on all four sublevels from rotational spectroscopy. Because of the anharmonic resonances pertaining to the low-*K* levels and the huge and irregular shifts of the most strongly influenced rotational transitions, the extensions of the rotational assignments were quite often ambiguous. This can be illustrated by the Fortrat diagram shown in Fig. 4 with a selection of some of the strongly perturbed series of transitions in the overtone level $v_{10} = 3$. Such a representation of a series of rotational transitions is a useful tool for propagating assignments in rotational spectra towards higher *J* values in spectra with only local resonances, like e.g. in one of the earlier analyses [10]. In our present case, however, perturbations have a global character and affect the series in a very irregular way. This made the assignment of the most perturbed series ambiguous, also because of the frequency gaps of the available submillimeter wave sources. Such ambiguities were removed by several iterations of extending the assignments of the IR spectra and checking the consistency of effective *B*, D_J and H_J constants of series of transitions belonging to the same *K* in both types of spectra. Finally, we arrived at a consistent set of data with which, however, we were not able to reproduce the observed transition frequencies in a fully quantitative manner [6]. Therefore we decided to proceed by

(i) extending the rotational measurement to higher *J*/*K* states to have a better balance of *J* values and
(ii) reanalyzing the lower levels involved in the corresponding hot bands ($v_{10} = 1$ and 2) with an account of all their anharmonic resonances.

Even when both of these steps were accomplished, we were not able to make the fit converge to within the experimental accuracy of the accurate rotational data. Thus we have to admit that a fully quantitative reproduction of the currently available data set is not possible without including the 1300-cluster in the rovibrational model. Doing that would require an extremely extensive study, with the problem of dealing with very weak infrared bands and vanishing intensities of the rotational transitions even more pronounced than in the current 1000-cluster.

The hot bands pertaining to the overtone and combination levels of the 1000-cluster were assigned from the spectra described in Section 2. Although we were not able to extend the assignments dramatically, with the aid of the new Loomis–Wood program with LSCD checking adapted now also for treatment of general hot bands, we approximately doubled the amount of IR data. Altogether we gathered almost 2000 transitions to the C0 (A_1+A_2) sublevel and almost 2500 transitions pertaining to the C2 (E) sublevel. For the overtone level, we now have over 1500 transitions in the $v_{10} = 3^{\pm1} \leftarrow 2^0$ bands and almost 1800 transitions in the $v_{10} = 3^{\pm3} \leftarrow 2^{\pm2}$ bands available. Also the body of rotational data pertaining to the combination and overtone levels has been more than doubled, containing more than 400 transitions in each of them.

In the least-squares fits, we used a Hamiltonian analogous to that used previously [6], extended by the anharmonic couplings

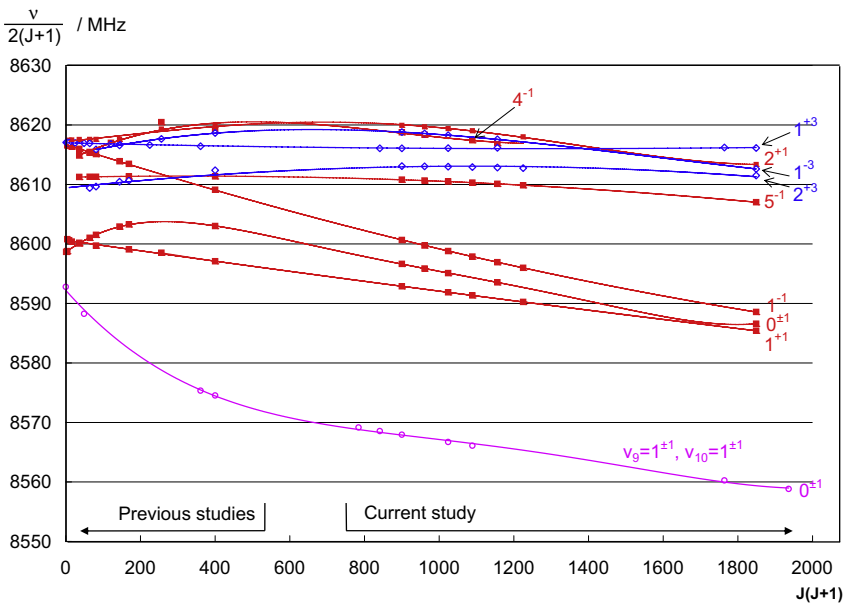

Fig. 4. Fortrat diagram of several low-K series of the rotational transitions in the $v_{10} = 3$ vibrational state. The transitions belonging to the O1 and O3 sublevels are marked with ■ and ◇ symbols, respectively. The lowermost series, marked with ○, belongs to the $K = 0$ transitions in the C2 level, which is perturbed by a local anharmonic resonance with $K = 0$ of O1.

to the 650-cluster and the q_{12} resonance described in the previous subsection. We thus have a set of resonances within the levels of the combination and overtone states (B, C, and I) in addition to those already present in the study of the 650-cluster (E, F, and G). It was our intention to reduce the effectivity of the latter by assigning transitions for the levels above these resonance crossings. The main obstacle for the case of resonances F and G were the very weak intensities for these high-K transitions of the hot bands, reaching the $v_{10} = 2^0$ and 2^{-2} levels, within the congested region of the v_{10} fundamental band. We were, however, more optimistic in the case of the resonance crossing E with the levels $v_9 = 1^{-1}$, for which the corresponding transitions were still reasonably strong. However, in this case we struggled with a different problem because they had very irregular patterns, for which the otherwise very efficient method of LSCD-assisted search was not of sufficient help because of the overlaps of these weaker lines with the much stronger ones in the highly congested region of the IR spectra. At this point we estimated the potential influence of the approaching level $v_9 = 2^{+2}$, not from the neighbor 1000-cluster but the higher 1300-cluster. Although we estimate this crossing (H) to occur for $K = 20$, the effect of this coupling (analogous to resonance D in the progression of the v_{10} levels) penetrates quite deep down into the $v_9 = 1^{-1}$ level and competes with resonance E. This can explain the high degree of effectivity of the coupling term of resonance E. The coincidence of resonances F and I with the latter being neglected leads to the effectivity of the former and perhaps also of the resonance term G. It may also contribute to the anomalies of the ratio of resonance terms B and C which differs significantly from the expected vibrational dependence [9].

As the fitted anharmonic terms E, F, G between the 650- and 1000-clusters changed with respect to the fit of the 650-cluster [8], we had to refine the parameters of the $v_9 = 1$ and $v_{10} = 2$ levels again. The change of the terms E, F, G is also due to the inclusion of an additional anharmonic term pertaining to the block of the vibrations of $A_1 + A_2$ symmetry (resonance Za in Fig. 1). This interaction, which connects only the A_1 levels of the combination state C0 ($A_1 + A_2$) with the level O2 (A_1), does not lead to any resonance crossing. Yet it turned out to be of considerable importance for fitting the data of the C0 level, because it probably balances the effect of another non-resonant interaction with O3 ($A_1 + A_2$), from which only the $v_{10} = 3^{+3}$ sublevel crosses the levels of C0. On the other hand, it is somewhat surprising in this context that the reproduction of data has not been sensitive almost at all to another anharmonic interaction that couples the A_1 levels of C0 with F5 (resonance Zb in Fig. 1), a level being much closer to C0 than O0. Releasing the C0-F5 interaction term led to divergence of the fit and we were able to find only a very shallow minimum by changing it stepwise, with only a marginal effect on improving the fit. Therefore, we finally decided to exclude it from our model.

In this global fit, the parameters of the F9 level changed only marginally within their statistical error limits. The change of parameters in the O2 sublevel was slightly larger, while considerable change occurred for the parameters of O0 because of introducing the additional anharmonic term (Za). For these two states, we refined the lower-order parameters and kept fixed some higher-order ones (to the values from the previous study [8]) with maintaining the reproduction of data in the 650-cluster practically identical. The parameters of the F10 level could be kept fixed without any change of reproduction of its data in the present global fit.

The neglected anharmonic resonances (I, K, L, and O–Zb) are obviously behind the problems of the good reproduction of higher-K data in the combination and overtone levels. In some cases, like in the fundamental levels, we had to give them zero-weights in the fits to maintain an acceptable reproduction of the lower-K levels. It also causes a general deficit of accuracy in the reproduction of the rotational data, whose accuracy is 2–5 times better than the average standard deviation of reproduction. However, it should be repeatedly pointed out that the consistency of IR and rotational data pertaining to the common series of levels from the 1000-cluster confirms the correctness of the assignments.

As a consequence of the neglected anharmonic interactions for $K \geqslant 10$, we were not able to remove the highly effective character of two important second-order Coriolis interactions between the combination and overtone levels, occurring for values of K just below. One of them brings into resonance the $K = 8$ and 9 levels of

Table 2
Energies, rotational and centrifugal distortion parameters[a] (cm^{-1}) of the vibrational ground state and the $v_5 = 1$ level.

Parameter	$v = 0$[b]	$v_5 = 1$ (F5)
E	0.0	930.276 530 (21)
A	5.308 312 9	5.300 964 6 (26)
B	0.285 059 768 3	0.283 800 493 (11)
$D_J \times 10^7$	0.980 422	1.024 005 (80)
$D_{JK} \times 10^6$	5.450 958	5.630 334 (239)
$D_K \times 10^5$	9.701 5	9.696 5 (74)
$H_J \times 10^{15}$	−2.227	263.97 (189)
$H_{JK} \times \times 10^{11}$	3.050 3	1.781 5 (66)
$H_{KJ} \times 10^{10}$	1.769 1	−7.504 6 (237)
$H_K \times 10^9$	0.0	−2.700 (539)
$L_{JJK} \times 10^{15}$	−0.210 5	0.0[b]
$L_{JK} \times 10^{15}$	−1.451	0.0[b]
$L_{KKJ} \times 10^{15}$	−13.55	0.0[b]

[a] Numbers in parentheses are one standard deviation in units of the last significant digit.
[b] Constrained values.

$v_9 = 1^{-1}$, $v_{10} = 1^{+1}$ with $K = 7$ and 8 of $v_{10} = 3^{-1}$, the other the $K = 10$ level of $v_9 = 1^{-1}$, $v_{10} = 1^{-1}$ with $K = 9$ of $v_{10} = 3^{-3}$. Another second-order Coriolis interaction connects the $v_8 = 1$ level with the combination level $v_9 = v_{10} = 1$. Although it does not have a resonant character, it could not be neglected because of the significantly worse reproduction of data. It effectively absorbs the effects of the other neglected interactions and its value also has to be regarded as effective.

In the overtone and combination levels, there is also a rich variety of l-type interactions. Besides the common q_t ($\Delta k = \pm 2$, $\Delta l = \pm 2$) interaction, there are higher order ones, which are described in the Appendix. Their role in improving the fits is indispensable because the anharmonic resonances at low values of K (B, C, I, M) produce strong irregularities of the level spacings and in that case these higher-order interactions cannot be absorbed well into the effective constants of the diagonal Hamiltonian matrix elements in Eq. (A1). Their values still carry a certain degree of effectivity due to the persisting effective representation of the anharmonic interactions. The q_t terms, on the other hand, are not affected in this way so much, which is demonstrated by their expected closeness to the values from the lower levels $v_9 = 1$ and $v_{10} = 1, 2$.

The effectivity of the vibration–rotation Hamiltonian is also the reason for the quite irregular values of some sextic centrifugal distortion parameters (H and τ). They can take values different from those in the previous analyses and obviously also from the ground state. Their statistical errors have been considerably reduced with respect to the previous study, which is because of the extension of especially the rotational data to higher J values (approximately from 20 to 40). Those which continued to have exceedingly small values and large statistical errors were rather constrained to zero, without any pronounced effects on data reproduction. The fitted parameters of the effective Hamiltonian are summarized in Tables 2–5. The details of the data reproduction are available in the Supplementary material accompanying this paper and also upon request from one of the authors (P.P.).

5. Conclusions

The present work represents a further step in analyzing the levels of propyne around 1000 cm^{-1}. It reveals the crucial role of anharmonic resonances in the coupling of all the vibrationally excited levels. The origin of anharmonic couplings is in the flexibility of the bending motions of the C—C≡C chain, which bring all the polyads together into one global system. Because we have studied this polyad of levels without the coupling terms to the next higher polyad, we could not avoid the effectivity of the rovibrational Hamiltonian used in the present analysis. This effectivity is the cause of the problems with a fully quantitative reproduction of the extremely accurate rotational data, which represent the main new experimental contribution of the present study. A consistent

Table 3
Energies, rotational, centrifugal distortion, and l-type parameters[a] (cm^{-1}) of the vibrational levels $v_9 = 1$, $v_{10} = 1$ and 2.

Parameter	$v_9 = 1$ (F9)	$v_{10} = 1$ (F10)[b]	$v_{10} = 2^0$ (O0)	$v_{10} = 2^{\pm 2}$ (O2)
E	638.575 214 (13)	330.947 033	650.935 790 (503)	671.352 180 (122)
A	5.307 002 8 (5)	5.306 248 1	5.305 552 1 (39)	5.303 108 5 (15)
B	0.285 232 739 5 (33)	0.285 858 285 6	0.286 645 124 (296)	0.286 640 253 1 (32)
$D_J \times \times 10^7$	0.984 296 (20)	1.006 233	1.001 376 (177)	1.032 042 (24)
$D_{JK} \times 10^6$	5.449 793 (64)	5.471 159	5.486 909 (190)	5.485 091 (76)
$D_K \times 10^5$	9.701 62 (51)	9.676 4	9.653 2 (82)	9.626 9 (37)
$H_J \times 10^{14}$	−11.040 4 (379)	0.624 1	4.597 8 (843)	0.753 8 (507)
$H_{JK} \times 10^{11}$	2.930 1 (16)	3.043 7	3.031 0 (35)	3.054 3 (21)
$H_{KJ} \times 0^{10}$	1.460 5 (41)	1.750 7	2.620 0 (247)	2.104 3 (83)
$H_K \times 10^9$	0.0[b]	0.0	15.577 (666)	2.741 (365)
$L_{JJK} \times 10^{16}$	−0.648 6[b]	−2.204	−1.686[b]	−2.345[b]
$L_{JK} \times 10^{15}$	5.907[b]	−1.279	−7.280[b]	−4.905[b]
$L_{JKK} \times 10^{14}$	11.114[b]	0.804	−54.958[b]	19.052[b]
$A\zeta$	5.306 886 7 (14)	4.733 914 5		4.734 186 7 (36)
$\eta_J \times 10^5$	1.553 285 (50)	1.116 879		1.124 678 (32)
$\eta_K \times 10^4$	3.954 38 (47)	3.647 89		3.639 47 (146)
$\tau_J \times \times 10^5$	0.0[b]	−1.078 2		0.0[b]
$\tau_{JK} \times 10^9$	−0.708 7 (52)	1.85		−1.237 5 (61)
$\tau_K \times 10^8$	0.0[b]			−2.389 (264)
$\sigma_{JK} \times 10^{14}$	0.0[b]			2.64[b]
$\sigma_{KJ} \times 10^{12}$	0.0[b]			−2.01[b]
$q_t \times 10^4$	−3.008 459 3 (84)	−5.600 291 7		−5.598 354 (45)
$q_{t,J} \times 10^9$	0.744 7 (23)	1.849 3		1.851 6 (14)
$q_{t,K} \times 10^7$	−3.233 2 (39)	1.588 1		1.610 8 (18)
$q_{t,JJ} \times 10^{14}$	−1.521[b]	−1.072		−1.072[b]
$q_{t,JK} \times 10^{12}$	1.242[b]	−0.986		−0.986[b]
$f_{44} \times 10^{12}$				8.857[b]

[a] Numbers in parentheses are one standard deviation in units of the last significant digit.
[b] Constrained to values from Ref. [8].

Table 4
Energies, rotational, centrifugal distortion, and *l*-type parameters[a] (cm^{-1}) of the vibrational levels $v_8 = 1$, $v_9 = v_{10} = 1$, and $v_{10} = 3$.

Parameter	$v_8 = 1$ (F8)	$v_9 = 1^{\pm1}$, $v_{10} = 1^{\mp1}$ (C0)	$v_9 = 1^{\pm1}$, $v_{10} = 1^{\pm1}$ (C2)	$v_{10} = 3^{\pm1}$ (O1)	$v_{10} = 3^{\pm3}$ (O3)
E	1036.147 539 (20)	960.842 992 (208)	980.289 098 (22)	980.296 108 (122)	1021.168 197 (181)
A	5.335 651 1 (37)	5.306 467 7 (43)	5.303 635 9 (26)	5.302 677 5 (39)	5.298 432 2 (45)
B	0.284 867 785 (138)	0.286 030 345 (176)	0.286 018 368 (59)	0.287 435 365 (37)	0.287 404 016 (25)
$D_J \times 10^7$	0.990 001 (113)	1.002 581 (147)	1.004 869 (123)	1.069 781 (146)	1.059 549 (100)
$D_{JK} \times 10^6$	5.421 429 (1167)	5.516 388 (759)	5.404 962 (634)	5.503 619 (527)	5.496 058 (411)
$D_K \times 10^4$	1.131 9 (12)	0.984 1 (19)	0.980 8 (8)	1.035 8 (10)	1.015 0 (19)
$H_J \times 10^{14}$	−1.469 (265)	−16.215 (320)	−1.543 (290)	14.015 (309)	0.0[b]
$H_{JK} \times 10^{11}$	1.543 (16)	5.284 (18)	2.992 (10)	2.215 (17)	3.132 (17)
$H_{KJ} \times 10^{10}$	2.533 (53)	5.490 (98)	6.937 (66)	−5.526 (55)	2.867 (51)
$H_K \times 10^8$	−1.143 (77)	1.025 (239)	−1.256 (118)	0.0[b]	−5.904 (329)
$A\zeta$	2.191 787 9 (39)	−0.567 782 8 (88)	10.035 102 8 (59)	4.734 154 5 (91)	4.733 446 2 (33)
$\eta_J \times 10^5$	0.110 072 (1093)	−0.212 970 (318)	2.618 608 (450)	1.140 226 (405)	1.134 616 (137)
$\eta_K \times 10^4$	3.356 0 (54)	−0.597 8 (116)	7.729 5 (92)	4.132 7 (111)	3.685 3 (48)
$\tau_J \times 10^{10}$	1.876 1 (107)	−1.200 0 (94)	0.0	0.481 3 (90)	0.236 8 (101)
$\tau_{JK} \times 10^9$	−4.234 (130)	12.494 (72)	−11.071 (65)	7.781 (46)	−1.799 (17)
$\tau_K \times 10^7$	6.984 (188)	1.479 (180)	2.062 (142)	−0.767 (222)	3.118 7 (105)
$q_t \times 10^4$	−1.456 59 (203)	−3.183 16 (93)[c]	−5.715 09 (103)[d]	−5.601 26 (23)	
$q_{t,J} \times 10^9$	−1.281 (14)	0.480 (17)[c]	0.799 (11)[d]	1.825 (3)	
$q_{t,K} \times 10^7$	29.47 (44)	−3.234[b,c]	1.588[b,d]	2.260 (22)	
$f_{24} \times 10^7$		−1.749 (81)		−0.885 (40)	
$f_{44} \times 10^{10}$		1.557 (3)			
R_l		1.872 25 (22)			−0.026 01 (40)
$R_{l,J} \times 10^5$		−1.833 (18)			
$R_{l,K} \times 10^8$		−4.65 (63)			

[a] Numbers in parentheses are one standard deviation in units of the last significant digit.
[b] Constrained values.
[c] Corresponds to the q_t^9 operator.
[d] Corresponds to the q_t^{10} operator.

Table 5
Interaction parameters[a] (cm^{-1}) between the studied vibrational states.

Parameter			Parameter		
$W_{F10,O2}$		1.726 02[c]	$W_{F5,O3}$	N	0.446 57 (17)
$W^J_{F10,O2} \times 10^5$	D[b]	−1.144 1[c]	$W^J_{F5,O3} \times 10^5$		−2.755 (74)
$W^{JJ}_{F10,O2} \times 10^{10}$		−1.316[c]	$W_{O0,C0}$	Za	−1.036 (31)
$W_{F9,O2}$	A	0.284 00[c]	$W^J_{O0,C0} \times 10^4$		7.38 (2)
$W^J_{F9,O2} \times 10^5$		−1.239 5[c]	$B^{\zeta y}_{\zeta F9,F10} \times 10^4$	A7a	6.613 [c]
$W_{C2,O1}$	B	0.235 34 (2)	$B^{\zeta y,J}_{\zeta F9,F10} \times 10^9$		9.71 [c]
$W^J_{C2,O1} \times 10^6$		−2.778 (64)	$B^{\zeta y}_{\zeta F9,O2} \times 10^4$	A7b	−6.486 [c]
$W_{C0,O3}$	C	0.451 57 (46)	$B^{\zeta y}_{\zeta C02,O13} \times 10^3$	A7c–e	1.025 (7)
$W^J_{C0,O3} \times 10^6$		−9.525 (44)	$B^{\zeta y}_{\zeta F8,C0} \times 10^2$	A8	−1.1105 (36)
$W_{F9,C2}$	E	1.257 20 (25)	$B^{\zeta y}_{\zeta F8,O1} \times 10^2$	A9	−3.199 (78)
$W_{O2,O1}$	F	3.522 4 (95)	$q_{12} \times 10^5$	A10	5.094 (16)
$W_{O0,O3}$	G	2.653 7 (69)	$q^J_{12} \times 10^9$		−1.71 (10)
$W_{F8,O1}$	J	1.502 07 (17)	$\alpha^{BB}_{F5,F8} \times 10^5$	A11	1.842 (12)
$W^J_{F8,O1} \times 10^5$		−6.590 (11)	$\alpha^{BB}_{F8,C0} \times 10^7$		−9.67 (5)

[a] Numbers in parentheses are one standard deviation in units of the last significant digit.
[b] Labels of anharmonic resonances (see Figs. 1 and 2) or equations in Appendix A.
[c] Constrained values.

simultaneous analysis with the rovibrational data is, however, a sound confirmation of their correct assignments.

Acknowledgments

This work was supported by the Grant Agency of the Academy of Sciences of the Czech Republic (projects IAA400400706 and IAA400400504) and the Ministry of Education, Youth and Sports of the Czech Republic (research program LC06071). The work in Köln was supported initially by the Deutsche Forschungsgemeinschaft (DFG) via the collaborative research grant SFB 494. More recently, support of HSPM has been provided by the Bundesministerium für Bildung und Forschung (BMBF), administered by Deutsches Zentrum für Luft- und Raumfahrt (DLR).

Appendix A. Definition of matrix elements of the effective vibration–rotation Hamiltonian

Although the definitions of the matrix elements of the effective vibration–rotation Hamiltonian employed in the calculations of the energy levels have appeared already in previous studies [7,8], we prefer to summarize them here with some additional comments. The diagonal matrix elements up to the sixth order are the conventional ones for a prolate C_{3v} symmetric-top molecule

$$E^0_{vr}(J,k,l) = E_v + B_vJ(J+1) + (A_v - B_v)k^2 - D^v_JJ^2(J+1)^2 - D^v_{JK}J(J+1)k^2 - D^v_Kk^4 + H^v_JJ^3(J+1)^3 + H^v_{JK}J^2(J+1)^2k^2 + H^v_{KJ}J(J+1)k^4 + H^v_Kk^6 + \left[-2A\zeta_v + \eta^v_JJ(J+1) + \eta^v_Kk^2 + \tau^v_JJ^2(J+1)^2 + \tau^v_{JK}J(J+1)k^2 + \tau^v_Kk^4\right]kl. \quad \text{(A1)}$$

Obviously, the third line of equation (A1) vanishes for the non-degenerate vibrational level F5 with $l = 0$. In the combination level $v_9^{l_9} + v_{10}^{l_{10}}$, there are four possible sign combinations of the two vibrational angular momentum quantum numbers l_t, i.e. $l_9 = -l_{10} = \pm 1$ (C0, with vibrational symmetry A_1+A_2) or $l_9 = l_{10} = \pm 1$ (C2, vibrational symmetry E). In this case, each l_t combines with its own $A\zeta$ constant (and its higher-order expansion terms $\eta_J, \ldots$), and these two contributions are subsequently summed in Eq. (A1). In order to use Eq. (A1) for the combination level, we used in place of $A\zeta$ "effective" constants $A\zeta^{eff}$, multiplied by the actual value of l_{10} of the particular sublevel of $v_9^{l_9} + v_{10}^{l_{10}}$. This means that the $A\zeta^{eff}$ constants of C0 and C2 are close to the combinations of $A\zeta$ constants of the fundamental levels, i.e. $A\zeta^{eff}_{C0} \sim -A\zeta_9 + A\zeta_{10}$ and $A\zeta^{eff}_{C2} \sim A\zeta_9 + A\zeta_{10}$, respectively. These effective $A\zeta, \eta_J, \ldots$ constants are those listed in Table 4.

For the C0 sublevels, these z-Coriolis terms are not the only source of splitting. The other contribution to A_1/A_2 splitting comes from the vibrational l-type resonance operator used here in the form

$$\langle v_9 = 1^{+1}, v_{10} = 1^{-1}; J, k|(\widehat{H}_{40} + \widehat{H}_{42})/hc|v_9 = 1^{-1}, v_{10} = 1^{+1}; J, k\rangle = R^{C0}_l + R^{C0}_{l,J}J(J+1) + R^{C0}_{l,K}k^2. \quad \text{(A2a)}$$

An analogous operator contributes to the splitting in the O3 sublevel

$$\langle v_{10} = 3^{-3}; J, k|\widehat{H}_{60}/hc|v_{10} = 3^{+3}; J, k\rangle = R^{O3}_l. \quad \text{(A2b)}$$

The q_{22} l-type operator has been used in the "Cartwright-Mills" form extended to higher order terms

$$\langle v^{l\pm 2}; J, k \pm 2|(\widehat{H}_{22} + \widehat{H}_{24})/hc|v^l; J, k\rangle = -\frac{1}{4}[(v \mp l)(v \pm l + 2)]^{1/2}\{q^v_t + q^v_{t,J}J(J+1) + q^v_{t,K}[k^2 + (k \pm 2)^2]\}F^{\pm}_2(J,k). \quad \text{(A3)}$$

This notation with the inclusion of the v,l-dependent factors is convenient here because the consistency of the constants with a different number of vibrational quanta excited, which is a measure of the good convergence of the effective Hamiltonian, can be easily checked. In the $v_9 = v_{10} = 1$ combination level, there are in fact two such operators corresponding to $\Delta l_9 = \pm 2$ and $\Delta l_{10} = \pm 2$.

The higher-order l-type operators used in the current study are of two types with $\sum \Delta l = \pm 4$

$$\langle v_9 = 1^{\pm 1}, v_{10} = 1^{\pm 1}; J, k \mp 2|\widehat{H}_{42}/hc|v_9 = 1^{\mp 1}, v_{10} = 1^{\mp 1}; J, k\rangle = 4f^{C02}_{24}F^{\mp}_2(J,k) \quad \text{(A4)}$$

and

$$\langle v_{10} = 2^{\pm 2}; J, k \pm 4|\widehat{H}_{44}/hc|v_{10} = 2^{\mp 2}; J, k\rangle = 8f^{O2}_{44}F^{\pm}_4(J,k) \quad \text{(A5a)}$$

$$\langle v_9 = 1^{\pm 1}, v_{10} = 1^{\pm 1}; J, k \pm 4|\widehat{H}_{44}/hc|v_9 = 1^{\mp 1}, v_{10} = 1^{\mp 1}; J, k\rangle = 4f^{C02}_{44}F^{\pm}_4(J,k) \quad \text{(A5b)}$$

$$\langle v_{10} = 3^{\pm 3}; J, k \pm 4|\widehat{H}_{44}/hc|v_{10} = 3^{\mp 1}; J, k\rangle = 8\sqrt{3}f^{O13}_{44}F^{\pm}_4(J,k). \quad \text{(A5c)}$$

In contrast to the l-type operator in Eq. (A3), these operators have their v,l-dependent factors given explicitly.

In the case of the anharmonic terms, the v,l-dependent factors are not included in the general matrix elements

$$\langle v; J, k|(\widehat{H}_{n0} + \widehat{H}_{n2})/hc|v'; J, k\rangle = W_{vv'} + W^J_{vv'}J(J+1) + W^K_{vv'}k^2, n = 3, 4. \quad \text{(A6)}$$

This means that the ratios of the fitted values should be close to the corresponding v,l-factors in the sequence of interactions $v_{10} = 1/2$, 2/3. However, a considerable deviation from these theoretical ratios were observed because of the still effective nature of the $v_{10} = 2/3$ interactions. Therefore, it was more convenient to fit the Fermi terms independently, not having the ratios constrained by the explicit v,l-factors.

The Coriolis interactions included in the present study were

$$\langle v_9 = 1^{\mp 1}, v_{10} = 0; J, k \pm 1|(\widehat{H}_{21} + \widehat{H}_{23})/hc|v_9 = 0, v_{10} = 1^{\pm 1}; J, k\rangle = \mp 2[B\zeta^y_{F9,O2} + B\zeta^{yJ}_{F9,O2}J(J+1)]F^{\pm}_1(J,k) \quad \text{(A7a)}$$

$$\langle v_9 = 0, v_{10} = 2^{\pm 2}; J, k \pm 1|\widehat{H}_{31}/hc|v_9 = 1^{\pm 1}, v_{10} = 0; J, k\rangle = \pm 2\sqrt{2}B\zeta^y_{F9,O2}F^{\pm}_1(J,k) \quad \text{(A7b)}$$

$$\langle v_9 = 0, v_{10} = 3^{\pm 1}; J, k \pm 1|\widehat{H}_{31}/hc|v_9 = 1^{\mp 1}, v_{10} = 1^{\pm 1}; J, k\rangle = \pm 2\sqrt{2}B\zeta^y_{C02,O13}F^{\pm}_1(J,k) \quad \text{(A7c)}$$

$$\langle v_9 = 0, v_{10} = 3^{\pm 1}; J, k \mp 1|\widehat{H}_{31}/hc|v_9 = 1^{\pm 1}, v_{10} = 1^{\pm 1}; J, k\rangle = \mp 2\sqrt{2}B\zeta^y_{C02,O13}F^{\mp}_1(J,k) \quad \text{(A7d)}$$

$$\langle v_9 = 0, v_{10} = 3^{\pm 3}; J, k \pm 1|\widehat{H}_{31}/hc|v_9 = 1^{\pm 1}, v_{10} = 1^{\pm 1}; J, k\rangle = \pm 2\sqrt{6}B\zeta^y_{C02,O13}F^{\pm}_1(J,k) \quad \text{(A7e)}$$

and

$$\langle v_9 = 1^{\mp 1}, v_{10} = 1^{\mp 1}; J, k \mp 1|\widehat{H}_{31}/hc|v_8 = 1^{\pm 1}; J, k\rangle = \mp 2B\zeta^y_{F8.C0}F^{\pm}_1(J,k) \quad \text{(A8a)}$$

$$\langle v_9 = 1^{\pm 1}, v_{10} = 1^{\pm 1}; J, k \pm 1|\widehat{H}_{31}/hc|v_8 = 1^{\pm 1}; J, k\rangle = \pm 2B\zeta^y_{F8.C0}F^{\pm}_1(J,k). \quad \text{(A8b)}$$

and

$$\langle v_{10} = 1^{\mp 1}; J, k \pm 1|\widehat{H}_{41}/hc|v_8 = 1^{\pm 1}; J, k\rangle = \mp 2B\zeta^y_{F8.O1}F^{\pm}_1(J,k). \quad \text{(A9)}$$

The resonance between F5 and $v_{10} = 2^{-2}$ is treated as a vibrationally off-diagonal analogue of the q_{12} l-type interaction

$$\langle v_5 = 0, v_{10} = 2^{\mp 2}; J, k \pm 1|(\mathbf{H}_{22} + \mathbf{H}_{24})/hc|v_5 = 1, v_{10} = 0; J, k\rangle = 2\{[q_{12} + q^l_{12}J(J+1)](2k \pm 1)\}F^{\pm}_1(J,k). \quad \text{(A10)}$$

The matrix element of the α-resonance between F5 and F8 has the form

$$\langle v_5 = 0, v_8 = 1^{\mp 1}; J, k \pm 2|\mathbf{H}_{22}/hc|v_5 = 1, v_8 = 0^0; J, k\rangle = 1/(2\sqrt{2})\alpha^{BB}_{F5,F8}F^{\pm}_2(J,k). \quad \text{(A11)}$$

The α-resonance between F8 and the C0 levels is formally the same; it is only of a higher-order $\mathbf{H}_{32}$ and pertains to both sublevels $v_9 = 1^{\pm 1}$ $v_{10} = 1^1$.The matrix elements of the rotational shifting operators were conventionally taken as

$$F^{\pm}_n(J,k) = \prod_{i=1}^{n}[J(J+1) - (k \pm i \mp 1)(k \pm i)]^{1/2}. \quad \text{(A12)}$$

Appendix B. Supplementary data

Supplementary data for this article are available on ScienceDirect (www.sciencedirect.com) and as part of the Ohio State University Molecular Spectroscopy Archives (http://library.osu.edu/sites/msa/jmsa_hp.htm). Supplementary data associated with this article can be found, in the online version, at doi:10.1016/j.jms.2009.04.003.

References

[1] A. Coustenis, T. Encrenaz, B. Bézard, G. Bjoraker, G. Graner, M. Dang-Nhu, E. Arié, Icarus 102 (1993) 240–260.
[2] P.M. Solomon, K.B. Jefferts, A.A. Penzias, R.W. Wilson, Astrophys. J. 168 (1971) L107.
[3] H.S.P. Müller, S. Thorwirth, L. Bizzocchi, G. Winnewisser, Z. Naturforsch. 55a (2000) 491–494.
[4] G. Graner, G. Wagner, J. Mol. Spectrosc. 144 (1990) 389–415.
[5] P. Pracna, J. Demaison, G. Wlodarczak, A. Lesarri, G. Graner, J. Mol. Spectrosc. 177 (1996) 124–133.
[6] P. Pracna, G. Graner, J. Cosléou, J. Demaison, G. Wlodarczak, V.-M. Horneman, M. Koivusaari, J. Mol. Spectrosc. 206 (2001) 150–157.
[7] H.S.P. Müller, P. Pracna, V.-M. Horneman, J. Mol. Spectrosc. 216 (2002) 397–407.
[8] P. Pracna, H.S.P. Müller, S. Klee, V.-M. Horneman, Mol. Phys. 102 (2004) 1555–1568.
[9] G. Graner, R. Farrenq, G. Blanquet, J. Walrand, K. Pekkala, J. Mol. Spectrosc. 161 (1993) 80–101.
[10] K. Pekkala, G. Graner, G. Wlodarczak, J. Demaison, J. Koput, J. Mol. Spectrosc. 149 (1991) 214–229.
[11] N.F. Henfrey, B.A. Thrush, J. Mol. Spectrosc. 113 (1985) 426–450.
[12] N.F. Henfrey, B.A. Thrush, J. Mol. Spectrosc. 121 (1987) 139–149.
[13] W.M. Rhee, J.A. Roberts, J. Mol. Spectrosc. 126 (1987) 356–369.
[14] W.M. Rhee, J.A. Roberts, J. Chem. Phys. 85 (1986) 6940–6944.
[15] H.S.P. Müller, B.J. Drouin, J.C. Pearson, L.R. Brown, I. Kleiner, A. Dehayem, J. Orphal, P. Chelin, R.L. Sams, Contribution WG03, presented at the 62nd International Symposium on Molecular Spectroscopy, June 18–22, Columbus, OH, USA, 2007.
[16] G. Winnewisser, A.F. Krupnov, M.Yu. Tretyakov, M. Liedtke, F. Lewen, A.H. Saleck, R. Schieder, A.P. Shkaev, S.V. Volokhov, J. Mol. Spectrosc. 165 (1994) 294–300.
[17] G. Winnewisser, Vib. Spectrosc. 8 (1995) 241–253.
[18] S. Brünken, H.S.P. Müller, F. Lewen, G. Winnewisser, Phys. Chem. Chem. Phys. 5 (2003) 1515–1518.
[19] H.S.P. Müller, S. Brünken, J. Mol. Spectrosc. 232 (2005) 213–222.
[20] A.G. Maki, J.S. Wells, in: Wavenumber Calibration Tables from Heterodyne Frequency Measurements, NIST Special Publication 821, US Government Printing Office, Washington, DC, 1991, p. 20402.
[21] (a) T. Ahonen, P. Karhu, V.-M. Horneman, An optimized White-type gas cell for the Bruker IFS 120 high resolution FTIR spectrometer, in: Fifteenth Colloquium on High Resolution Molecular Spectroscopy, Glasgow, Scotland, 8–13 September, 1997.;
(b) http://physics.oulu.fi/irspe/Sivut/cell40-2002.pdf.
[22] V.-M. Horneman, R. Anttila, J. Pietilä, S. Alanko, M. Koivusaari, J. Mol. Spectrosc. 229 (2005) 89–107.
[23] P. Pracna, K. Sarka, J. Demaison, J. Cosléou, F. Herlemont, M. Khelkhal, H. Fichoux, D. Papoušek, M. Paplewski, H. Brger, J. Mol. Spectrosc. 184 (1997) 93–105.
[24] W. Lodyga, M. Kreglewski, P. Pracna, Š. Urban, J. Mol. Spectrosc. 243 (2007) 182–188.
[25] G. Graner, J. Demaison, G. Wlodarczak, R. Anttila, J. Hillman, D.E. Jennings, Mol. Phys. 64 (1988) 921–932.
[26] R. Bocquet, W.D. Chen, D. Papoušek, G. Wlodarczak, J. Demaison, J. Mol. Spectrosc. 164 (1994) 456–472.